ELSEVIER

Journal of Alloys and Compounds 216 (1994) 273–280

Journal of ALLOYS AND COMPOUNDS

Structural investigation of the metastable compound A1 in an as-cast Fe–Nd eutectic alloy

J. Delamare, D. Lemarchand*, P. Vigier

Groupe de Métallurgie Physique de Rouen, Unité de Recherche associée au CNRS 808, 76821 Mont Saint Aignan Cedex, France

Received 25 March 1994; in final form 9 May 1994

Abstract

In this paper some structural and chemical informations about the compound A1 are given. Transmission electron microscopy investigations reveal that it is composed of a mixture of two nanocrystalline compounds A1α and A1β, with atomic compositions close to $Nd_{20}Fe_{80}$ and $Nd_{40}Fe_{60}$, respectively. Their formation is described in a metastable phase diagram including also $NdFe_2$, and is confirmed by thermodynamic calculations on the basis of Miedema's model.

Keywords: Iron; Neodymium; Transmission electron microscopy

1. Introduction

The microstructure of sintered Nd–Fe–B permanent magnets consist of large grains of the ferromagnetic $Nd_2Fe_{14}B$ phase, surrounded by an Nd-rich intergranular phase. Some precipitates of the paramagnetic phase $Nd_{1.1}Fe_4B_4$ are localized at the triple-grain-junction boundaries. The Nd-rich phase results from the solidification of the terminal liquid in the course of the post-sintering cooling process. Its composition is in the neighbourhood of the ternary Nd-rich eutectic, indicated as E_2 in the Nd–Fe–B liquidus projection given by Matsuura et al. [1]. The composition of the Nd-rich phase is not clearly established at the moment, particularly because of its chemical reactivity and its low volume fraction (less than 10% in a typical magnet $Nd_{15}Fe_{77}B_8$ at.%). The similarities in composition and solid–liquid transition temperature of the ternary eutectic E_2 and the binary eutectic Fe–Nd (e_8 from [1]) led us to use the binary eutectic alloy as representative for both eutectic alloys.

Since the observation by Drozzina and Janus [2] of a high and unexplained coercivity in as-cast Fe–Nd alloys, several workers [3–5] have demonstrated the existence of a new phase called A1 in such alloys, which was also found in some ternary Fe–Nd–B alloys [4–6]. All studies confirm that this phase is metastable and ferromagnetic with a Curie temperature of 245 °C, and that it possesses a large magnetic anisotropy. The structure and composition reported in these studies are collected in Table 1. They show a large spread in values. In order to obtain a more precise understanding of the structure and of the mechanism at the origin of the stabilization of the phase A1, an as-cast Nd–Fe eutectic alloy have been studied by transmission electron microscopy (TEM).

2. Experimental details

The starting material was a commercial as-cast Nd–Fe eutectic alloy (Johnson Mattey Businness Inc.), of 99.9% purity. We investigated the microstructure of the ingot using a JEOL JSM 35 CF scanning electron microscope. Structural data of the phases present were obtained by X-ray diffraction (Cu Kα radiation) and by electron diffraction with a JEOL 2000 FX II (accelerating voltage, 200 kV) transmission electron microscope. For the TEM observation, specimens were thinned to electron transparency by combining electropolishing and Ar ion milling at 5 keV. We obtained the same results whatever the thinning process used. The chemical composition of phases was measured with a LINK energy-dispersive X-ray microanalysis system (Si detector) associated to the microscope. Owing to the expansion of the beam inside the thinned sample, the chemical composition is measured in a cylinder with a diameter less than 100 nm. The length of this cylinder corresponds to the thickness of the sample.

*Corresponding author.

SSDI 0925-8388(94)01271-I

Table 1
Characteristic of the phase A1 determined by several workers, as well as the kind of Nd–Fe alloy used to observe the phase A1

Reference	Composition of A1	Structure of A1	Material studied
[3,4]	$NdFe_4+O$	Unknown	As-cast eutectic Fe–Nd
[7]	$NdFe_4+O$	Lattice spacing: 0.254 nm, 0.256 nm 0.193 nm and 0.165 nm	As-cast eutectic Fe–Nd and Melt-spun eutectic Fe–Nd
[8]	Nd_6Fe_{23}	Cubic; $a=0.152$ nm	Melt-spun Fe–Nd
[9]	Heteregeneous; NdFe (TEM) between $NdFe_3$ and $NdFe_{2.6}$ (Mössbauer)	Nanocrystalline; lattice spacings 0.235 nm and 0.203 nm	As-cast eutectic Fe–Nd
[10]	Nd_3Fe_7	Tetragonal; $a=0.80$ nm, $c=1.19$ nm	As-cast and melt-spun Fe–Nd
[11]	$NdFe_{1.1}$	Unknown	Fe–Nd–B

The coercivity measurements were performed at room temperature using a vibrating-sample magnetometer, and thermomagnetic scans were performed using a Faraday balance, in magnetic flux densities up to 1.5 T. The Curie temperature was determined by the minimum of dM/dT.

3. Results

3.1. Microstructural investigation

In accordance with [4,9,12], two kinds of eutectic morphology can be identified in the as-cast Nd–Fe eutectic alloy (Fig. 1(a)). The first consists of lamellae of the ferromagnetic phase Nd_2Fe_{17} ($T_C=55$ °C), embedded in an α-Nd (d.h.c.p. structure) matrix. The second is the fine-grained eutectic described by Schneider et al. [4] and by Givord et al. [13] (Fig. 1(b)). It consists of an arrangement of two phases: the ferromagnetic compound A1 ($T_C=245$ °C) and metallic α-Nd, each appearing to be continuous. The coercivity that we have measured in this alloy ($H_c=0.36$ MA m^{-1}) is in good agreement with previous values [2], and results from the occurrence of the compound A1. The two kinds of eutectic morphology are metastable; they transform into the final equilibrium phases $Nd+Nd_5Fe_{17}$, in accordance with the Nd–Fe phase diagram redrawn by Landgraf et al. [14].

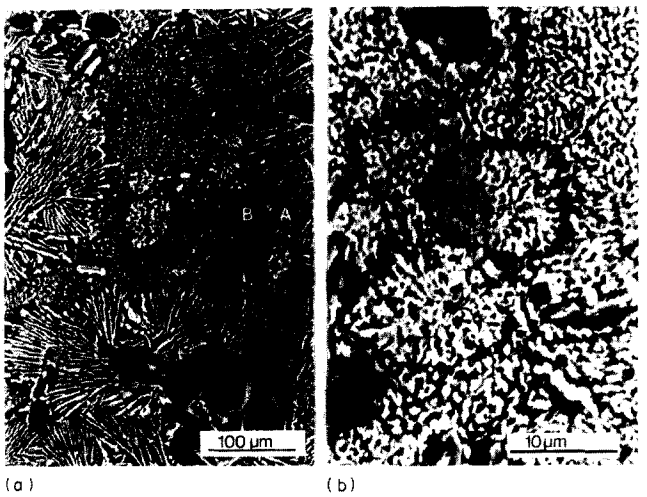

Fig. 1. (a) Scanning electron micrograph of a eutectic Nd–Fe alloy showing the two kinds of eutectic morphology: A, lamellar eutectic constituted of Nd_2Fe_{17} (bright) and α-Nd (dark); B, globular eutectic constituted of A1 (bright) and α-Nd (dark). (b) Zoom image of the globular eutectic showing the bicontinuous overlapping of A1 and Nd.

3.2. Chemical composition

Energy-dispersive X-ray spectra acquired by TEM reveal the presence of Nd, Fe and a small amount of O in the compounds A1 (Fig. 2). However, the oxygen detected seems to result from the thinning process, since the O Kα peak also appears on the surface of Nd_2Fe_{17} and Nd_5Fe_{17}, whatever the thinning process

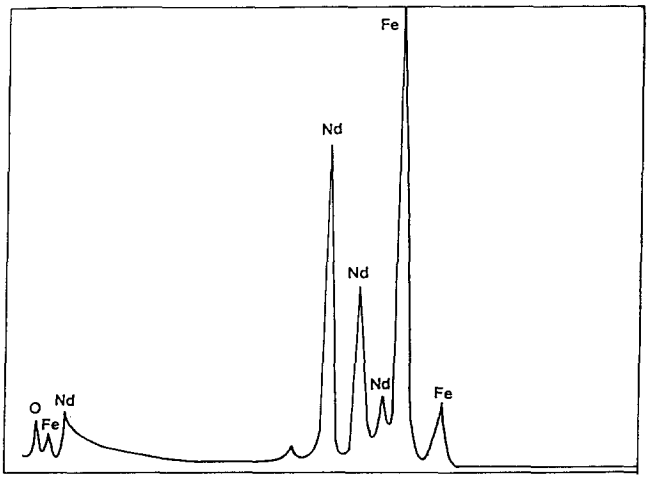

Fig. 2. Energy-dispersive X-ray spectrum of the phase A1: O Kα peak results of the thinning process.

used [15]. Except for O Kα, no additional peak is detected. We therefore believe that the compound A1 is a purely binary Fe–Nd phase.

TEM and energy-dispersive X-ray investigations of A1 reveal that this compound consists of the association of two complex submicron structures (Fig. 3(a)). For the first, large bright areas (about 100 nm large) with an approximate atomic composition $Nd_{20}Fe_{80}$ (compound A1α) are embedded in a continuous dark area (less than 50 nm) in which the Nd content is in the range 20–40 at.%. The second structure, occurring together with the first, contains large dark regions with an approximate atomic composition $Nd_{40}Fe_{60}$ (compound A1β) and is embedded in a continuous bright area having the same Nd content of 20–40 at.%. So it is clear that A1 consist of a combination of these two compounds, A1α and A1β, as shown in the schematic drawing in Fig. 3(b). The continuous area could be considered as a mixture of A1α and A1β.

These results explain those of Givord et al. [13]. Their TEM investigations indicate that the phase A1 is heterogeneous on a scale of 10 nm. The chemical compositions measured by several workers [3,5,7,13] can be regarded as a combination of the compositions of the two compounds A1α and A1β and has an Nd content within the range 20–40 at.%.

3.3. Structural study

Selected-area electron diffraction patterns were obtained with a selection aperture of 200 nm so that it was difficult to distinguish between structural information from both compound A1α and compound A1β. The two compounds cannot be differentiated by the dark-field method, owing to the vicinity and the width of the amorphous rings, as seen in Fig. 3(c).

Three kinds of ring are identified. The first is composed of a series of three rings associated with the presence of microcrystalline Nd_2O_3–C particles probably formed during the thinning process. They were used as internal standards for the measurement of the other lattice spacing with an accuracy better than 2%. The second kind is a large and intense halo (the corresponding lattice spacing is in the range 0.279–0.324 nm), which can be associated with an amorphous neodymium oxide. Its occurrence was also observed in association with other intermetallic compounds such as Nd_2Fe_{17}. The third kind of ring is associated with the compounds A1α and A1β. The lattice spacings and their width are indicated in Table 2. Using the Scherrer formula $L = (0.89\lambda)/(\Delta \cos \theta)$ (where Δ is the half-height width of the peaks), the correlation length L is 1 nm. This value is close to the value determined by

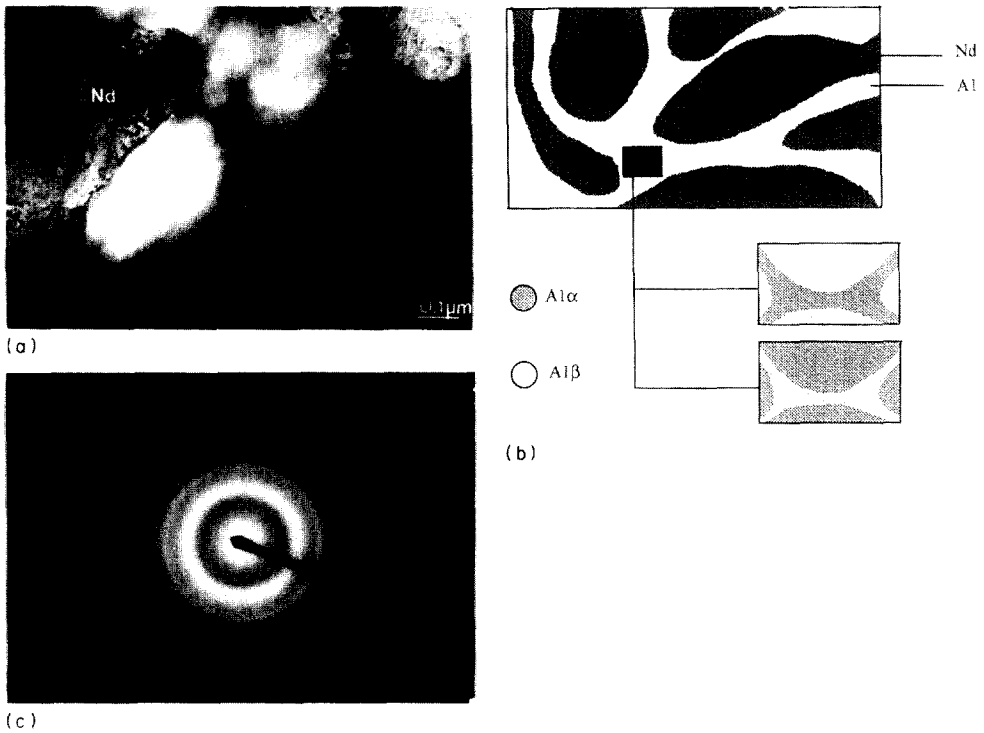

Fig. 3. (a) Electron micrograph of A1, corresponding to grains of A1α (bright) embedded in an A1β matrix (dark). (b) Schematic drawing of the A1 + Nd globular eutectic. On the micrometre scale, one observes a globular eutectic constituted of Nd and A1 whereas, on a submicronic scale, A1 appears to be constituted of A1α and A1β. (c) Electron diffraction of A1 showing also the presence of microcrystalline Nd_2O_3-C and amorphous neodymium oxide. The width of the amorphous rings associated with A1 leads to a correlation length of 10 Å, characteristic of a nanocrystalline compound.

Table 2
Values of the lattice spacing and broadening of the diffuse rings corresponding to the phase A1

Mean lattice spacing (nm)	Broadening of the rings (nm)	Relative broadening (%)
0.213	0.0040	1.9
0.166	0.0035	2.1
0.146	0.0035	2.4
0.124	0.0025	2.0

Givord et al. [13] by neutron diffraction in an as-cast $Nd_{80}Fe_{20}$ sample.

The sample was heated in situ in the transmission electron microscope under a vacuum of 10^{-8} Torr. The temperature range was 20–600 °C. A typical oxidation process occurs above 370 °C, leading to the formation of microcrystalline α-Fe and Nd_2O_3-A. The occurrence of α-Fe as a first product of the oxidation process indicates that the phase A1 is actually a mixture of intermetallic compounds, and not a mixture of oxides.

4. Description of the formation mechanism of the compounds A1α and A1β using a metastable phase diagram

The metastable phase diagram shown in Fig. 4, including the compound $NdFe_2$, is relevant to explain the formation mechanism of the compounds A1α and A1β. Three experimental features are taken into account to describe its formation.

First, the metastable compound A1 is present only in the binary Nd-Fe and Pr-Fe systems, whereas the occurrence of A1 was not reported in the other R–Fe systems (with R ≡ rare earth). This experimental situation can be related to the stabilization of the Laves phase RFe_2 for the latter systems. So, we can assume an intimate relation between the occurrence of the compound A1 and the absence of the Laves phases $NdFe_2$ and $PrFe_2$.

Second, the intermetallic phase $NdFe_2$ can be solidified under special conditions; its occurrence as a metastable phase is confirmed by earlier observations, which indicate the presence of $NdFe_2$ in melt-spun alloys [8,16], or in as-cast alloys when impurities are introduced [12,17]. Then, the solidification of $NdFe_2$ as a metastable phase is not to be excluded in as-cast eutectic alloys, owing to the low value of the melting point of the eutectic alloys.

Third, the chemical compositions of A1α and A1β are located on each side of $NdFe_2$ in the phase diagram, suggesting that these phases can result from decomposition of $NdFe_2$.

Based on these three experimental considerations, the metastable phase diagram in Fig. 4 includes $NdFe_2$, A1α and A1β. The regions of metastability of these phases are indicated by the broken lines (i.e. "high" temperature for $NdFe_2$ and low temperature for A1α and A1β). In the following discussion, we shall consider, for simplicity, that the two compounds A1α and A1β are stoichiometric, with respective compositions $NdFe_4$ and Nd_2Fe_3.

According to Oswald's [18,19] rule, "it is not the most stable state with the lowest free energy which is initially obtained, but the least stable lying nearest to the original state in free energy". In other words, if several metastable states are possible between the initial and final states, they will consecutively be formed corresponding to decreasing free energy. Thus the solidification of an Nd–Fe liquid close to the eutectic composition will lead firstly to the metastable equilibrium state according to

$$L \longrightarrow Nd + NdFe_2$$

as explained above. Owing to the metastable character of $NdFe_2$, it tends again to decompose into A1α and A1β, following the reaction

$$5NdFe_2 \longrightarrow NdFe_4(A1\alpha) + 2Nd_2Fe_3(A1\beta) \quad (1)$$

During a short-time anneal at 600 °C of the sample, the phases A1α and A1β are not stable and decompose into Nd_2Fe_{17} and free Nd [4], following the reactions

$$17NdFe_4(A1\alpha) \longrightarrow 4Nd_2Fe_{17} + 9Nd \quad (2)$$

$$17Nd_2Fe_3(A1\beta) \longrightarrow 3Nd_2Fe_{17} + 28Nd \quad (3)$$

This third intermediate state is also metastable. During another anneal at 600 °C, the participating phases transform to the final equilibrium state consisting of Nd(79.9 at.%) + Nd_5Fe_{17}(20.1 at.%), as confirmed by several workers [4,14]. The final equilibrium state is in accordance with the stable phase diagram redrawn by Landgraf et al. [14]. The formation mechanism that we propose is the same as for the Pr–Fe system.

The absence of A1 in the R–Fe systems with R ≡ Sm to Lu results from the fact that RFe_2 is a stable phase in these systems. Thus we can conclude that the formation of A1 proceeds via the formation of RFe_2 as a metastable phase; the only R-Fe systems which satisfy this condition are Nd–Fe and Pr–Fe.

5. Thermodynamic calculation of the stability sequence of the R–Fe compounds with the help of Miedema's model

Following Oswald's rule, the successive phase transformations occurring during the solidification of the eutectic Nd–Fe liquid correspond to a progressive decrease in the free energy of the resulting compounds. We have used the thermodynamic model of Miedema to calculate these free energies. We shall discuss first

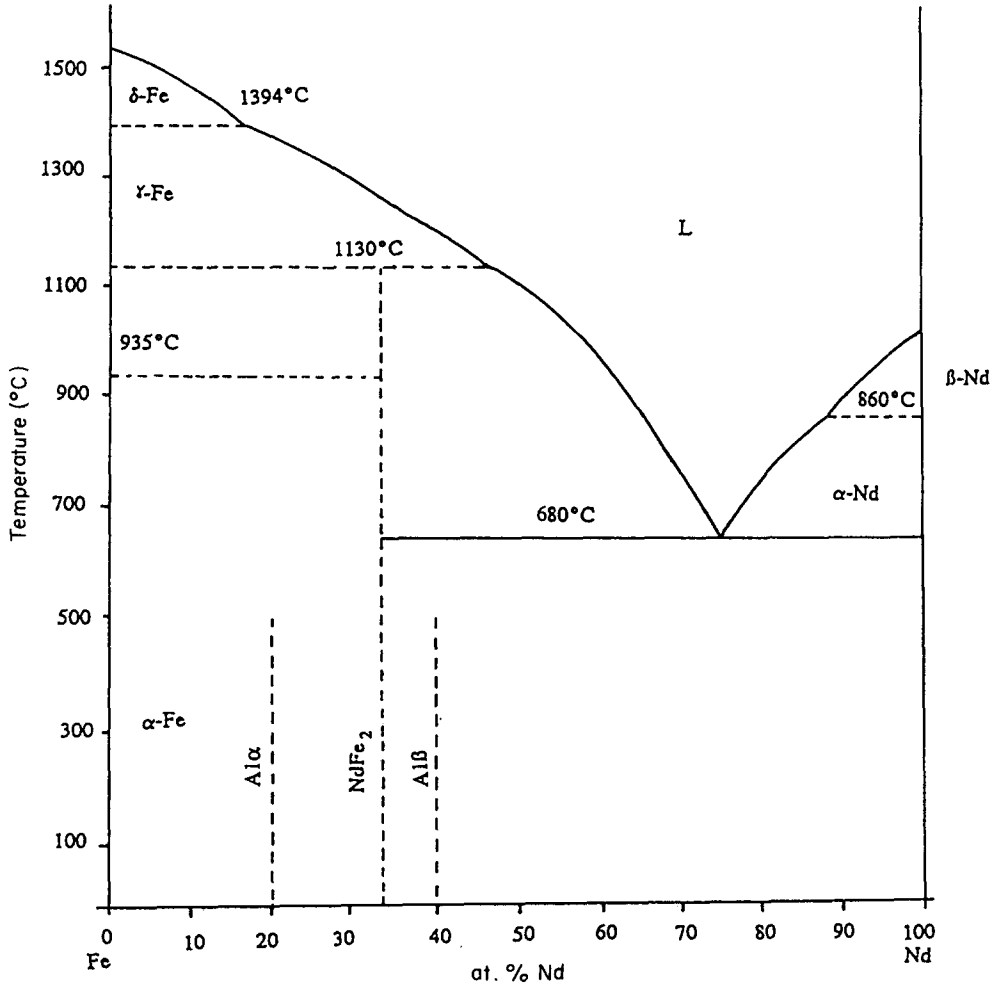

Fig. 4. Fe–Nd metastable phase diagram including three metastable phases: $NdFe_2$, A1α and A1β. In the course of the solidification of an eutectic alloy, the metastable equilibrium state will be $NdFe_2$+Nd. However, $NdFe_2$ tends to decompose into A1α and A1β and leads to the metastable equilibrium Nd+A1α+A1β observed in this alloy.

the sequence of occurrence of stable R–Fe compound (R ≡ rare earth), and we shall show that $NdFe_2$ and $PrFe_2$ are metastable. Then, the successive steps of decomposition of $NdFe_2$, particularly the formation of A1α and A1β, will be ascertained in the framework of this model.

5.1. Enthalpy of formation and sequence of stabilization of R–Fe compounds

The stability of a compound is determined by the variation ΔG^{for} in the Gibbs free energy during the formation of the compound corresponding to the sum of two terms: ΔH^{for}, the enthalpy of formation of the compound which depends on the composition; $-T\,\Delta S^{for}$, the entropy contribution which, for solid compounds, is very small compared with ΔH^{for} and will be neglected [20].

ΔH^{for} can be estimated using the semiempirical model developed by Miedema [20]. In this model, three parameters per atom (the chemical potential ϕ^* for electronic charge, the electron density n_{WS} at the boundary of the Wigner–Seitz atomic cell and the molar volume V), and two empirical constants ($P = 14.2$ and $Q/P = 9.4$) are introduced. For concentrations C_A and C_B of atoms A and B in the compound, ΔH^{for} (expressed in kilojoules per mole of atoms) can be calculated using

$$\Delta H^{for} = 2C_A V_A^{2/3} C_B^S [1 + 8(C_A^S C_B^S)^2] P \times [-(\Delta\phi^*)^2 + (Q/P)(\Delta n_{WS}^{1/3})^2][n_{WS\,A}^{-1/3} + n_{WS\,B}^{-1/3}]^{-1} \quad (1)$$

where

$$\Delta n_{WS}^{1/3} = n_{WS\,A}^{1/3} - n_{WS\,B}^{1/3} \qquad \Delta\phi^* = \phi_A^* - \phi_B^*$$

$$C_A^S = \frac{C_A V_A^{2/3}}{C_A V_A^{2/3} + C_B V^{2/3}}$$

$$C_B^S = \frac{C_B V_B^{2/3}}{C_A V_A^{2/3} + C_B V_B^{2/3}} = 1 - C_A^S$$

The sign of the enthalpy of formation determining the stability of the compound is given by the sign of the expression inside the large parentheses:

$$\left(-(\Delta\phi^*)^2+\frac{Q}{P}(\Delta {n_{WS}}^{1/3})^2\right)$$

It is only dependent on the nature of the atoms A and B, and not on their concentration. The other part of Eq. (1) gives the value of ΔH^{for} as a function of the concentration. (ΔH^{for}) shows an extremum $(\Delta H^{for})_{ext}$ for a composition close to RFe_2 in the R–Fe series [21]. The curve of ΔH^{for} vs. concentration given in Fig. 5 for the Nd–Fe system was calculated using the parameters ϕ^*, n_{WS} and V given by Miedema [20] and Labulle [21]. In Table 3 we report the calculated values of the enthalpy of formation of the Laves phases RFe_2 in the corresponding R–Fe systems (R ≡ La to Lu), as well as the number of intermetallic phases in this system. By examining this table, we can deduce a sequence of stabilization of R-Fe intermetallic compounds when the enthalpy of formation decreases in the R–Fe series: R_2Fe_{17}, (R_5Fe_{17}), RFe_2, RFe_3, R_6Fe_{23}. The phase R_5Fe_{17} is indicated in parentheses because its stability in systems other than Nd–Fe and Pr–Fe has not been investigated until now. So we shall ignore this phase in the following discussion. Nevertheless, it has no consequence for the occurrence of the phase A1 in the R–Fe systems, owing to the long-time annealing heat treatment required for its solidification. The parameters ϕ^*, n_{WS} and V for Pr are very close to those for Nd. So, the same behavior is to be expected (and is generally observed) as in the Nd–Fe system.

According to Miedema's model, the small positive values of $(\Delta H^{for})_{ext}$ for the La–Fe, Pr–Fe and Nd–Fe systems indicate that the number of stable intermetallic compounds is reduced (i.e. no compound at all or only R_2Fe_{17}). On the contrary, the small positive value of $(\Delta H^{for})_{ext}$ for the Pr–Fe and Nd–Fe systems indicates that formation of metastable compounds can be expected. Looking at the sequence of stabilization of R–Fe intermetallic compounds described above, the

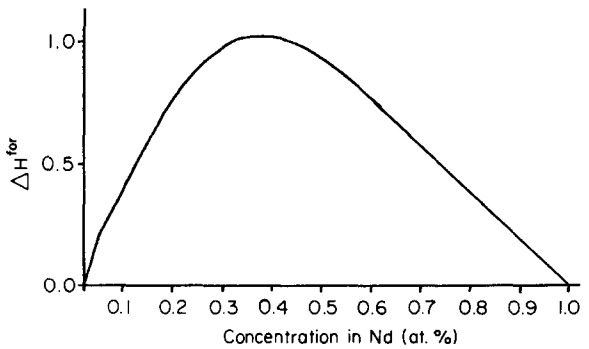

Fig. 5. Calculated curve of ΔH^{for} vs. concentration for the Nd–Fe solid solutions. This curve shows an extremum value for a composition close to $NdFe_2$, as do the other R–Fe systems.

Table 3
Number of intermetallic compounds in R–Fe systems related to the decreasing values of the enthalpy of formation of RFe_2 compounds (except for Ce–Fe and Yb–Fe systems, the number of intermetallic compounds increases when the enthalpy of formation decreases)

	Value for the following rare earths R													
	La	Ce	Pr	Nd	Sm	Gd	Ho	Tb	Dy	Yb	Tm	Er	Lu
Calculated enthalpy of formation of RFe_2 (kJ mol^{-1} of atom)	+6.70	−39.81	+1.00	+1.00	−1.69	−1.69	−2.97	−4.27	−4.27	−6.68	−6.70	−6.74	−10.36
Stable intermetallic compounds (experimental)		C_2Fe_{17}	Pr_2Fe_{17}	Nd_2Fe_{17}	Sm_2Fe_{17}	Gd_2Fe_{17}	Ho_2Fe_{17}	Tb_2Fe_{17}	Dy_2Fe_{17}	Yb_2Fe_{17}	Tu_2Fe_{17}	Er_2Fe_{17}	Lu_2Fe_{17}
		$CeFe_2$			$SmFe_2$	$GdFe_2$	$HoFe_2$	$TbFe_2$	$DyFe_2$		$TuFe_2$	$ErFe_2$	$LuFe_2$
			Pr_5Fe_{17}	Nd_5Fe_{17}									
					$SmFe_3$	$GdFe_3$	$HoFe_3$	$TbFe_3$	$DyFe_3$		$TuFe_3$	$ErFe_3$	$LuFe_3$
							Ho_6Fe_{23}	Tb_6Fe_{23}	Dy_6Fe_{23}	Yb_6Fe_{23}	Tu_6Fe_{23}	Er_6Fe_{23}	Lu_6Fe_{23}
Number of intermetallic compounds (experimental)	0	2	2	2	3	3	4	4	4	2	4	4	4

Table 4
Calculated values of the enthalpy of formation of RFe_2, RFe_4 and R_2Fe_3 compounds evaluated from Eq. (1) (the variation in enthalpy during reaction (1) is also given)

	Enthalpy of formation of the compound (kJ mol^{-1} of atom) for the following R											
	Ce	Pr	Nd	Sm	Gd	Ho	Tb	Dy	Yb	Tm	Er	Lu
RFe_2	−39.81	+1.00	+1.00	−1.69	−1.69	−2.97	−4.28	−4.26	−6.68	−6.70	−6.74	−10.36
$RFe_4(A1\alpha)$	−28.27	+0.75	+0.75	−1.26	−1.26	−2.18	−3.17	−3.14	−4.86	−4.88	−4.94	−7.52
$R_2Fe_3(A1\beta)$	−41.57	+1.01	+1.01	−1.72	−1.72	−3.05	−4.37	−4.36	−6.88	−6.89	−6.93	−10.68
Enthalpy of reaction	+40.1	−1.15	−1.15	+1.85	+1.85	+3.15	+4.65	+4.60	+7.10	+7.20	+7.10	+11.0

first metastable compound to be expected in Nd–Fe eutectic alloy is $NdFe_2$.

5.2. Compatibility of the formation mechanism of A1α and A1β with the thermodynamic calculation

In order to confirm that the reactions (1)–(3) (see Section 4) take place in the system Nd–Fe, we have calculated the variation in the enthalpy, denoted $(\Delta H^{for})_{R1}$, in the course of reaction (1), as indicated in [22]. It is given by the difference of the total enthalpy of formation of the constituents after and before the reaction (1), indicated by $(\Delta H^{for})_{R1}{}^{a}$ and $(\Delta H^{for})_{R1}{}^{b}$ respectively. Hence, we may write

$$(\Delta H^{for})_{R1}{}^{a} = +13.85 \text{ kJ} \quad (\Delta H^{for})_{R1}{}^{b} = +15.00 \text{ kJ}$$

and

$$(\Delta H^{for})_{R1} = (\Delta H^{for})_{R1}{}^{a} - (\Delta H^{for})_{R1}{}^{b} = -1.15 \text{ kJ}$$

The calculated values of $(\Delta H^{for})_{R1}$ for the other R–Fe systems (R ≡ Pr to Lu) are collected in Table 4. The La–Fe system is excluded, because of the high value of ΔH^{for} which inhibits the formation of $LaFe_2$ as a stable or metastable phase.

$(\Delta H^{for})_{R1}$ is negative in only two cases (namely Pr–Fe and Nd–Fe), indicating that reaction (1) may occur. In contrast, reaction (1) will be inhibited for the other systems, owing to the positive value of $(\Delta H^{for})_{R1}$. So, one has to expect the occurrence of the phase A1 only in the Nd–Fe and Pr–Fe systems, and the absence of this phase (and the stability of the Laves phase RFe_2) in other systems. This is fully confirmed by the experiment.

Using the same calculation, we can evaluate $(\Delta H^{for})_{R}$ for reactions (2) and (3) (i.e. the formation of Nd_2Fe_{17} from A1α and A1β) in the Nd–Fe system: $(\Delta H^{for})_{R2} = -29.2$ kJ for reaction (2); $(\Delta H^{for})_{R3} = -60.0$ kJ for reaction (3).

So, reactions (2) and (3) are likely to occur in the Nd–Fe system (and in Pr–Fe). The A1α and A1β phases are not stable phases, and they transform into Nd_2Fe_{17}, and later into Nd_5Fe_{17}, as indicated by Landgraf et al. [14].

6. Conclusion

On a microscopic scale, the compound A1 appears to be a globular eutectic in association with neodymium whereas, on a submicron scale, A1 is constituted of two nanocrystalline compounds A1α and A1β. Their atomic compositions were determined by energy-dispersive X-ray analysis and correspond to compositions close to $Nd_{20}Fe_{80}$ and $Nd_{40}Fe_{60}$ respectively. Structural information given by electron diffraction indicate that these compounds are nanocrystalline, with a correlation length of 1 nm. The formation mechanism of these two compounds can be explained using a metastable Nd–Fe phase diagram including $NdFe_2$ in addition to other stable or metastable compounds. In accordance with Oswald's rule, the solidification mechanism of an Nd–Fe eutectic alloy leads firstly to an Nd + $NdFe_2$ metastable equilibrium, secondly to A1α + A1β + Nd equilibrium by dissociation of $NdFe_2$, thirdly to Nd_2Fe_{17} + Nd by dissociation of A1α and A1β, and finally to the stable equilibrium state Nd_5Fe_{17} + Nd. Calculations of the variation in enthalpy associated with every transformation described above lead to negative values in all cases, confirming that these reactions occur in the Nd–Fe system. In contrast, the same calculations made for all systems other than Nd–Fe and Pr–Fe lead to positive values, which are associated with the stability of RFe_2, and to the absence of the A1 phase. This was experimentally confirmed by several studies.

References

[1] Y. Matsuura, S. Hirosawa, H. Yamamoto, S. Fujimura, M. Sagawa and K. Osamura, *Jpn. J. Appl. Phys., 24* (1985) L635.
[2] V. Drozzina and R. Janus, *Nature, 135* (1935) 36–37.
[3] G. Schneider, G. Martinek, H.H. Stadelmaier and G. Petzow, *Mater. Lett., 7* (1988) 215.
[4] G. Schneider, F.J.G. Landgraf and F.P. Missel, *J. Less-Common. Met., 153* (1989) 169–180.
[5] K.G. Knoch, *Thesis,* University of Stuttgart, 1990.
[6] K.J. Strnat, H.F. Mildrum, M. Tokunaga and H. Harada, *J. Appl. Phys., 63* (1988) 3321.
[7] G.C. Hadjipanayis, A. Tsoukatos and J. Strzeszewski, *J. Magn. Magn. Mater., 78* (1989) 169.

[8] L.X. Liao, Z. Altounian and D.H. Ryan, *J. Appl. Phys., 67* (9) (1990) 4821.
[9] J.P. Nozières, *Thesis*, University of Grenoble, 1990.
[10] J. Strzeszewski, A. Tsoukatos and G.C. Hadjipanayis, *J. Appl. Phys., 67* (9) (1990) 4966–4968.
[11] K.G. Knoch, B. Grieb, E.Th. Henig, H. Kronmüller and G. Petzow, *IEEE Trans. Magn., 26* (5) (1990) 1951.
[12] G. Schneider, E.-Th. Henig, G. Petzow and H.H. Stadelmaier, *Z. Metallkd., 78* (1987) 694.
[13] D. Givord, J.P. Nozieres, M.F. Rossignol, D.W. Taylor, I.R. Harris, D. Fruchart and S. Miraglia, *J. Alloys Comp., 176* (1991) L5.
[14] F.J.G. Landgraf, G. Schneider, V. Villas-Boas and F.P. Missel, *J. Less-Common Met., 163* (1990) 209.
[15] J. Delamare, *Thesis,* University of Rouen, 1992.
[16] C.J. Yang, S.D. Choi and W.Y. Lee, *J. Appl. Phys., 69* (9) (1990) 4821.
[17] N. Amri, *Thesis,* University of Rouen, 1993.
[18] W. Oswald, *Z. Phys. Chem., 22* (1897) 289–330.
[19] W. Oswald, *Grundriss der Allgemeinen Chemie,* Wilhelm Engelmann, Leipzig, 1899.
[20] F.R. De Boer, R. Boom, W.C.M. Mattens, A.R. Miedema and A.K. Niessen, in F.R. de Boer and D.G. Pettifor (eds.), *Cohesion in Metals,* Vol. 1, North-Holland, Amsterdam, 1983, pp. 13–92.
[21] B. Labulle, *Thesis,* University of Rouen, 1985.
[22] F.R. De Boer, R. Boom, W.C.M. Mattens, A.R. Miedema and A.K. Niessen, in F.R. de Boer and D.G. Pettifor (eds.), *Cohesion in Metals,* Vol. 1, North-Holland, Amsterdam, 1983, pp. 640–643.